R. J. Stango
Assistant Professor of Mechanical Engineering.
Assoc. Mem. ASME

S. M. Heinrich
Assistant Professor of Civil Engineering.
Assoc. Mem. ASME

C. Y. Shia
Graduate Research Assistant, Mechanical Engineering.

Marquette University,
1515 W. Wisconsin Avenue,
Milwaukee, WI 53233

Analysis of Constrained Filament Deformation and Stiffness Properties of Brushes

In this paper, an analytical procedure is developed for evaluating the filament loading, constrained elastic deformation, and overall stiffness of a circular brush. Filament deformation is computed on the basis of a large displacement mechanics analysis in conjunction with kinematic constraints for a flat, rigid workpart with smooth surface finish. Numerical results are reported which examine the relationship between workpart penetration, brush stiffness, and force distribution characteristics of the workpart contact zone.

1 Introduction

Wire brushes are commonly used for polishing, deburring, and for the expedient removal of surface substances. In previous years, such applications frequently involved the hand-regulated use of brushes and, apparently, little attention was given to the analysis of brush properties, performance, and material removal mechanics. Thus, limited technical information is available in the literature pertaining to the design and in-service performance of filamentary brush systems.

Recently developed brushing methods employ robotic systems for automated deburring and surface finishing applications [4, 8]. It is known that the brush stiffness, rotational speed, and force exerted on the workpart play a crucial role in establishing the material removal rate and surface finish quality. Thus, in order to ensure the accurate and efficient use of brushes in the computer-aided manufacturing process, a clear understanding of the brush stiffness properties and dynamic characteristics must be developed.

Brushing processes involve a complex filament-workpart interaction within a relatively narrow surface region. Contact forces are developed as the filament tip moves along a constrained path, as described by the workpart surface. Generally, large filament deformation can result due to the applied forces and subsequent brush penetration by the workpart. Although large displacement mechanics analyses have been the subject of investigation for several decades [1, 7, 9], the problem involving large deformation along a constrained path has apparently not yet been reported.

The present research examines the stiffness properties of circular brushes on the basis of a large displacement mechanics analysis. Constrained filament deformation is evaluated for circular brushes in contact with a flat, rigid workpart, and special attention is given to examining fundamental characteristics of the filament-workpart contact region. Frictional forces which are developed between the filament tip and workpart surface are omitted in the present study. The analysis assumes quasistatic filament contact with the workpart, and is based upon the following additional assumptions for the brush system: interaction between individual filaments is neglected; filaments emanate radially from the hub center and are uniformly distributed along the circumferential direction; brush eccentricity is neglected; filaments are initially straight, of equal length, and obey Hooke's law.

Contributed by the Production Engineering Division for publication in the JOURNAL OF ENGINEERING FOR INDUSTRY, Manuscript received July 1988; revised December 1988.

2 Mechanics Analysis of Filament Deformation and Brush Stiffness

An idealized geometry of a circular, filamentary brush, commonly used for deburring and polishing applications, is shown in Fig. 1. Each filament of the brush has constant circular cross-section and is assumed to be clamp-supported at the hub outside radius, $r = r_h$.

Deformation of a monofilament is examined in Fig. 2 for the case of quasistatic contact with a flat, rigid workpart. As the hub rotates counterclockwise, each filament has initial contact with the smooth surface S, at $\Omega = \Omega_C$, and subsequently undergoes large deflection while remaining in contact with the workpart, until final release angle Ω_R is reached. The dashed horizontal line located at $\Omega = 0$ corresponds to the free-filament length and, in conjunction with the surface S, defines brush penetration depth Δ.

Deformation of the i_{th} filament is illustrated in Fig. 3. Normal force F_i is shown at the contact point of the deformed filament on S, and, on the basis of large displacement mechanics analysis [5], the following nonlinear differential equation is obtained:

$$v_i'' = \frac{M_i}{EI}\,[1 + (v_i')^2]^{3/2}, \tag{1}$$

where M_i is the bending moment, v_i is the displacement along the y-axis and $(')$ denotes differentiation with respect to the position coordinate, u_i, for the displaced configuration. Thus, for the initially straight filament having normal and transverse force components shown, the following mathematical formulation of the problem is obtained:

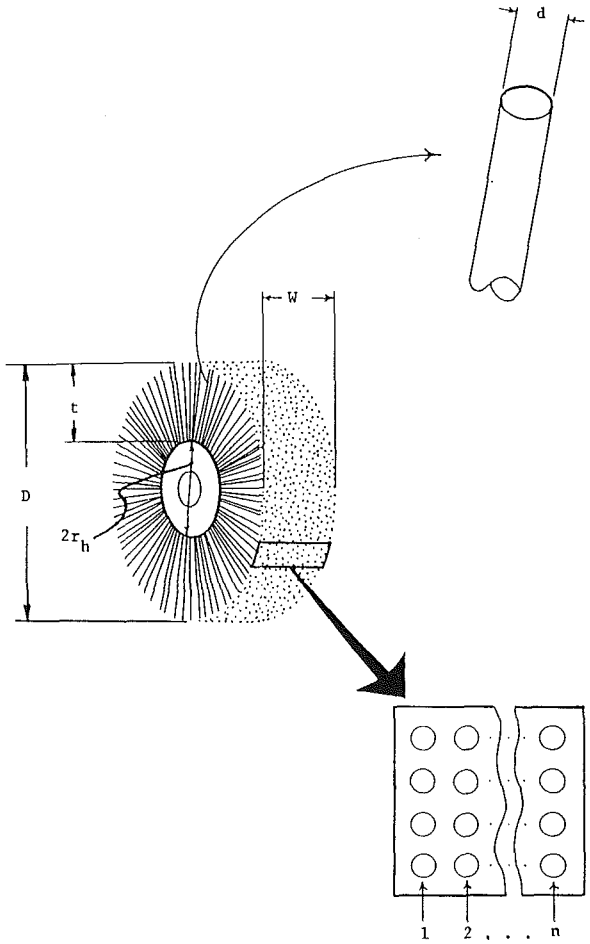

Fig. 1 Geometry of a circular filamentary brush

$$v_i''(u_i) = -\frac{F_i}{EI}\,[1+(v_i')^2]^{3/2}\,[\sin(\Omega_i)\,(u_i^*-u_i) - \cos(\Omega_i)\,(v_i(u_i^*)-v_i(u_i))], \tag{2}$$

with boundary conditions

$$v_i(0)=0, \tag{3}$$

$$v_i'(0)=0, \tag{4}$$

$$v_i''(u_i^*)=0, \tag{5}$$

along with the constraint

$$t=\int_0^{u_i^*}\sqrt{1+(v_i')^2}\,du_i, \tag{6}$$

where u_i^* and $v_i(u_i^*)$ correspond to the displacement solution of u_i and v_i on S, respectively, and t is the filament length. The constraint given by equation (6) is based upon the assumption that no axial deformation occurs along the filament length. The numerical solution of equations (2)–(6) involves a systematic approach for evaluating load F_i, deformation (u_i^*, $v_i(u_i^*)$) and corresponding filament angle Ω_i, and is further discussed in the next section. One may observe from the mathematical formulation of the problem, that a change in the filament flexural rigidity EI will only affect the solution by altering the end force F_i in direct proportion, that is,

$$\frac{F_i}{EI}=\text{constant}. \tag{7}$$

Thus, if a solution is obtained for $(EI)_1$, then the solution for $(EI)_2 \neq (EI)_1$ is also known. The two filament configurations are identical, while the forces at the filament tip are related by

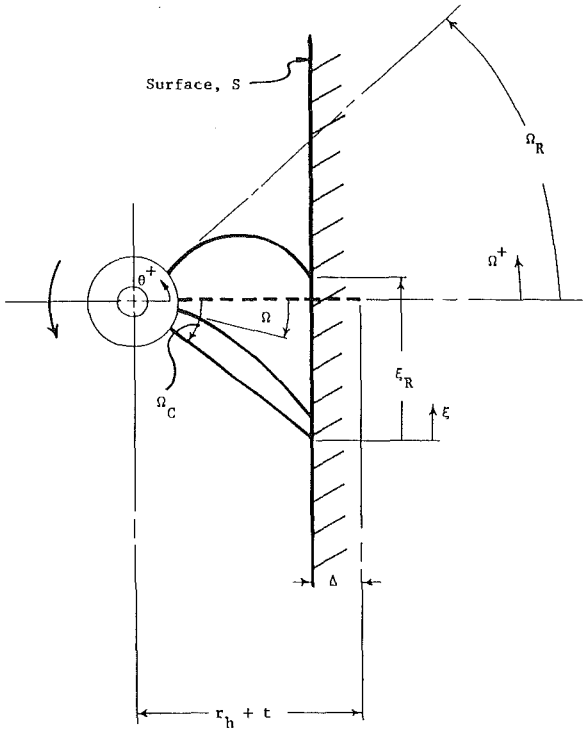

Fig. 2 Deformation of a single filament at the initial, intermediate, and release positions

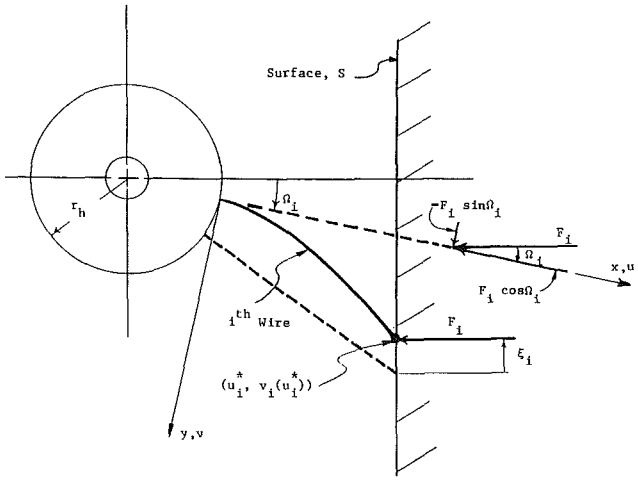

Fig. 3 Deflection of i_{th} filament and corresponding load for the deformed and undeformed configurations

$$(F_i)_2=\frac{(EI)_2}{(EI)_1}\,(F_i)_1. \tag{8}$$

The release angle Ω_R, can be obtained by noting that the filament bending moment at this configuration satisfies $M(0) = M(u_i^*) = 0$, as shown in Fig. 4. Thus, the filament geometry at the release position can be examined on the basis of large deformation column analysis, and the projected length l is [2, 10]

$$l=\frac{4E(p)}{k}-t, \tag{9}$$

where

$$k=\left(\frac{F_R}{EI}\right)^{1/2}=\frac{2G(p)}{t}, \tag{10}$$

$$p=\sin\left(\frac{\Omega_R}{2}\right), \tag{11}$$

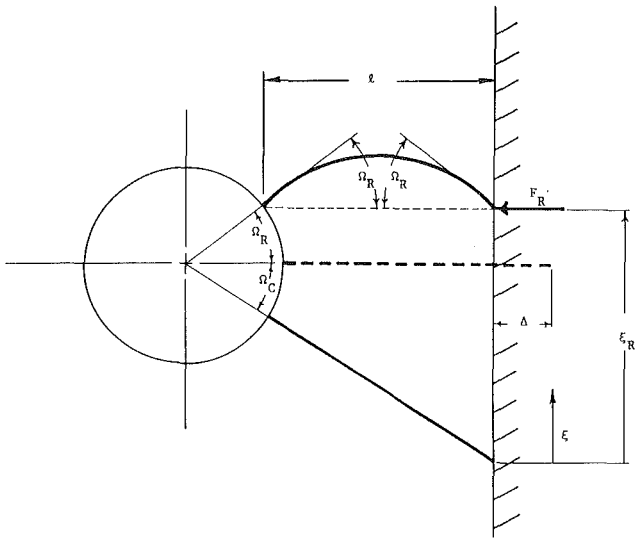

Fig. 4 Filament configuration at release position

and $G(p)$, $E(p)$ are complete elliptical integrals of the first and second kind, respectively. An accurate approximation of Ω_R can be obtained by using an iterative procedure which employs equations (9), (10), and (11), in conjunction with the geometric relationship

$$l = t - \Delta + r_h\,(1 - \cos(\Omega_R)), \tag{12}$$

and results in the release angle Ω_R and associated release load F_R for a specified brush penetration depth Δ. Evaluation of the release angle leads to the determination of the "contact zone," that is, the region over which the filament and workpart are in contact:

$$0 \le \xi \le \xi_R, \tag{13}$$

where

$$\xi_R = r_h \sin(\Omega_R) - (r_h + t)\sin(\Omega_C), \tag{14}$$

and

$$\Omega_C = -\cos^{-1}\left(1 - \frac{\Delta}{t + r_h}\right). \tag{15}$$

Thus, the extent of the contact zone is determined by the brush penetration depth Δ and the geometric properties of the filamentary brush system.

Brush stiffness K_j for a system of N uniformly spaced filaments along the hub circumference, having a brush penetration depth Δ_j, is evaluated by superposing individual loads, that is

$$K_j = \frac{\mathfrak{F}_{j+1} - \mathfrak{F}_{j-1}}{\Delta_{j+1} - \Delta_{j-1}}, \quad (j = 1,2, \ldots) \tag{16}$$

where

$$\mathfrak{F} = \sum_{i=1}^{m} F_i, \tag{17}$$

and m is the total number of filaments on S, such that $0 \le \xi_i \le \xi_R$, and F_i is the corresponding filament load. Stiffness property K_j is associated with a uniform distribution of filaments in a single plane and, therefore, overall stiffness $\mathcal{K}_j$ for a brush having n rows of aligned filaments, as shown in Fig. 1, is given by $\mathcal{K}_j = nK_j$. It is noted that the resultant force $\mathfrak{F}$ will vary with the rotation of the brush hub, due to progressive contact and release of filaments along ξ. It is further noted that, for a particular filament deformation, the proportionate relationship F_i/EI = constant is valid for any choice of flexural rigidity EI. Thus, numerical results for force and stiffness quantities are reported in the more useful forms, $\mathfrak{F}/EI$ and K/EI.

3. Solution Procedure for Evaluating Constrained Filament Deformation

In this section, the procedure used for obtaining numerical solutions for constrained filament deformation is examined. By employing the change of variables $g_1(u) = v(u)$ and $g_2(u) = v'(u)$, equation (2) is rewritten as

$$g_1'(u) = g_2(u), \tag{18}$$

$$g_2'(u) = -\frac{F}{EI}\,[1 + g_2^2(u)]^{3/2}[\sin(\Omega)(u^* - u) - \cos(\Omega)(v(u^*) - g_1(u))], \tag{19}$$

with boundary conditions

$$g_1(0) = 0, \tag{20}$$

$$g_2(0) = 0, \tag{21}$$

where subscript i has been dropped. In addition to satisfying the boundary conditions, it is required that numerical solutions to equations (18) and (19) be obtained for filament-workpart contact, that is, $(u, v) = (u^*, v(u^*))$ on S. Thus, the constrained deformation problem consists of an initially unknown relationship between filament angle Ω, filament load F, and filament displacement $(u^*, v(u^*))$.

The solution procedure used in the present research assumes a known filament position ξ on S, associated with the filament displacement

$$v(u^*) = (a - b - \xi)\cos(\Omega), \tag{22}$$

$$u^* = (t + r_h - \Delta)/\cos(\Omega) + v(u^*)\tan(-\Omega) - r_h, \tag{23}$$

where

$$a = (t + r_h)\sin(-\Omega_C), \tag{24}$$

$$b = (t + r_h - \Delta)\tan(-\Omega), \tag{25}$$

and employs an iterative procedure for obtaining F and Ω which, in addition to satisfying equations (18)–(21), also minimizes Ψ_i, $(i = 1, 2)$, where

$$\Psi_1 = |\, v(u^*) - g_1(u^*)\,|, \tag{26}$$

$$\Psi_2 = \left|\, t - \int_0^{u^*} \sqrt{1 + g_2^2(u)}\,du \,\right|, \tag{27}$$

where $v(u^*)$ is obtained by employing equation (22), and $g_1(u^*)$ is the corresponding result computed from the incremental numerical solution. Equation (26) is obtained by employing the boundary condition $M(u^*) = 0$, and equation (27) is derived from the assumption that the initial and deformed filament lengths are equal.

Numerical solutions for equispaced $\xi^{(k)}$, $(k = 1,2, \ldots)$ are obtained by employing fourth-order Predictor-Corrector equations in conjunction with a Runge-Kutta method [3, 6]. Initial guesses for Ω and F are obtained on the basis of a quadratic polynomial extrapolation procedure which uses previously obtained numerical solutions; for example

$$\Omega_{(1)}^{(k)} = 3(\Omega^{(k-1)} - \Omega^{(k-2)}) + \Omega^{(k-3)}, \quad (k \ge 4) \tag{28}$$

where $\Omega_{(1)}^{(k)}$ is the initial guess corresponding to the current position on the workpart, $\xi^{(k)}$. Successive $\Omega^{(k)}$ are obtained by employing the Secant Method [3]

$$\Omega_{n+1}^{(k)} = \Omega_n^{(k)} - \frac{1}{2}\left[\Psi_{2(n)}^{(k)}\,\frac{\Omega_n^{(k)} - \Omega_{n-1}^{(k)}}{\Psi_{2(n)}^{(k)} - \Psi_{2(n-1)}^{(k)}}\right], \quad (n = 2,3, \ldots) \tag{29}$$

along with a similar equation for evaluating filament loads, $F^{(k)}$. This procedure yields the successive reduction of Ψ_i, $(i = 1,2)$, and convergent solutions for $\Omega^{(k)}$ and $F^{(k)}$ are obtained by employing the parameters δ_i, such that $\Psi_i \le \delta_i$.

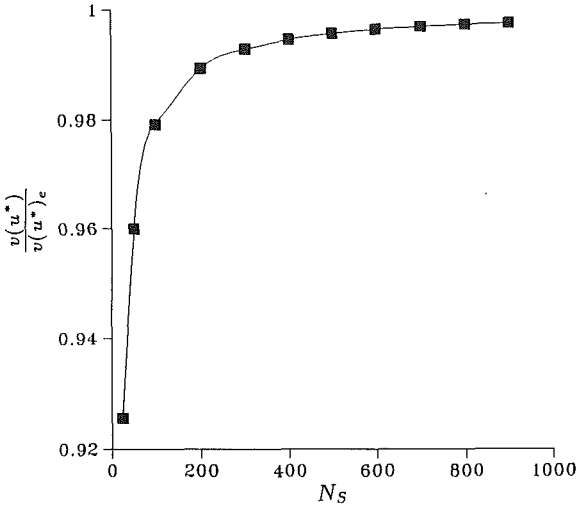

Fig. 5 Convergence characteristics for $(v(u^*)/v(u^*)_e)$ vs. number of iterative steps, N_s, with $\Omega = 0$ ($t/r_h = 1$, $\Delta = 0.508$ cm (0.2 in.))

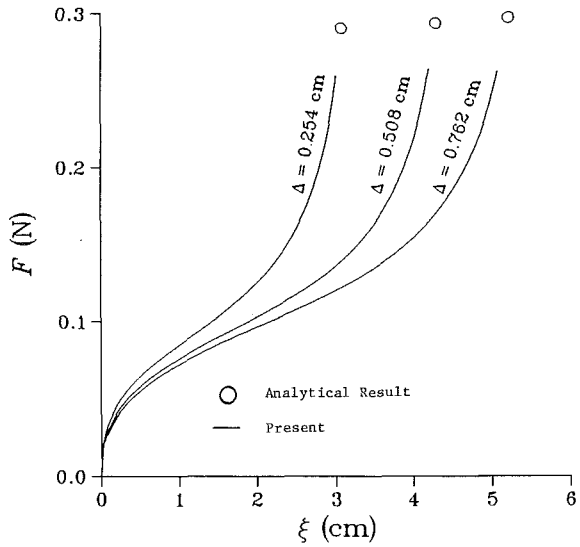

Fig. 6 Filament force F along ξ coordinate for $\Delta = 0.254$ cm (0.1 in.), 0.508 cm (0.2 in.), and 0.762 cm (0.3 in.), with $t/r_h = 1.0$

4 Results and Discussion

For the purpose of illustration, numerical studies are reported for wire brush systems having filament modulus of elasticity $E = 2.068 \times 10^2$ GPa (30×10^6 psi), filament diameter $d = 0.0254$ cm (0.01 in.), and overall brush diameter $D = 15.24$ cm (6.0 in.). Convergence parameters δ_i used throughout the investigation are given by $\delta_1 = 10^{-5}$ and $\delta_2 = 10^{-4}$, and numerical solutions are obtained which minimize equations (26) and (27) along with the additional requirement that $\Omega^{(k)} > \Omega^{(k-1)}$.

In Fig. 5, the nature and stability of convergent solutions for filament deformation $v(u^*)$ is examined for various numbers of steps, N_s, used in the incremental numerical procedure. Normalized solutions $\hat{v}(u^*) = v(u^*)/v(u^*)_e$ are reported for $\Omega = 0$, where $v(u^*)$ is the transverse displacement evaluated in the present research, and $v(u^*)_e$ is the corresponding exact solution obtained on the basis of post-buckling analysis [2, 10]. Transverse displacement $v(u^*)_e$ is obtained by employing the filament load F which was computed from the present research at $\Omega = 0$. Convergence studies for $t/r_h = 0.5$, 1.0, and 2.0 with arbitrary penetration depths, $\Delta = 0.254$ cm (0.1 in.), 0.508 cm (0.2 in.), and 0.762 cm (0.3 in.), yield approximately the same numerical result, and $N_s = 100$ is

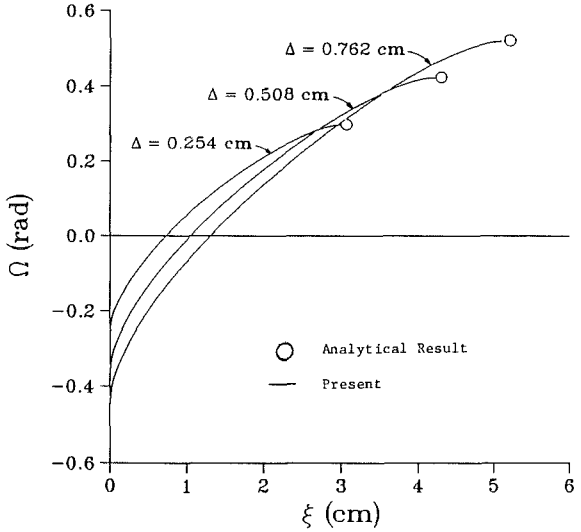

Fig. 7 Filament angle Ω vs. filament position along ξ for $\Delta = 0.254$ cm (0.1 in.), 0.508 cm (0.2 in.), and 0.762 cm (0.3 in.), with $t/r_h = 1.0$

employed for the numerical studies throughout the present research.

Magnitude of a single filament load F along the workpart contact zone ξ is examined in Fig. 6 for $t/r_h = 1.0$. Solid lines are used to illustrate the present numerical solutions for penetration depths $\Delta = 0.254$ cm, 0.508 cm, 0.762 cm (0.1 in., 0.2 in., 0.3 in., respectively), and open circles depict the filament release solutions (ξ_R, F_R), evaluated by employing large deformation column analysis. A large load gradient is observed at the initial and final contact positions of the filament. Final magnitudes of the filament loads at these penetration depths, however, are approximately constant for both the numerical results and exact solutions. Numerical solutions for the final filament contact positions along ξ are in excellent agreement with the results obtained by large deformation column analysis. Comparison of the final magnitude of the release force by the two different approaches yields a discrepancy of 11 percent.

The relationship between the filament angle Ω and the location of the filament tip $(u, v) = (u^*, v(u^*))$ along ξ is illustrated in Fig. 7 for $t/r_h = 1.0$, with penetration depths $\Delta = 0.254$ cm (0.1 in.), 0.508 cm (0.2 in.), and 0.762 cm (0.3 in.). Final contact angles obtained by the numerical solutions (terminal point of the solid lines) are in excellent agreement with the results computed by large deformation column analysis (open circles). The initial contact angles Ω_C, and release angles Ω_R, are obtained directly from the figure, and it is observed that, in general, $|\Omega_C| \neq |\Omega_R|$. Furthermore, it is noted that throughout the contact region ξ, $|d\xi/d\Omega|_{n+1} > |d\xi/d\Omega|_n$, $(n = 1,2, \ldots)$, with max $|d\xi/d\Omega|$ at $\xi = \xi_R$ and, therefore, an increased rate of filament tip displacement progressively occurs along ξ, as the brush hub undergoes steady rotation.

The distribution of filaments, $P = (1 - N_\xi/N_{\xi R})$, along the normalized contact zone, $\hat{\xi} = \xi/\xi_R$, is illustrated in Fig. 8 for a wire brush system having $N = 500$ equispaced filaments, $t/r_h = 1.0$, and penetration depth $\Delta = 0.508$ cm (0.2 in.). The designations N_ξ and $N_{\xi R}$ correspond to the number of filaments on S over the partial region $0 \leq \bar{\xi} \leq \xi$, and the contact zone, $0 \leq \bar{\xi} \leq \xi_R$, respectively, with initial filament contact at Ω_C. A very sparse filament distribution is noted in the vicinity of the release position, $\hat{\xi} = 1.0$. For example, the final 10 percent of the contact zone ($0.9 \leq \hat{\xi} \leq 1$), has fewer than two percent of the number of contact zone filaments, $N_{\xi R}$.

In Fig. 9, the extent of the contact zone ξ_R is examined for penetration depth $0 \leq \Delta \leq 0.762$ cm (0.3 in.), with $t/r_h = 0.5$, 1.0, and 2.0. In each case, the growth of the workpart

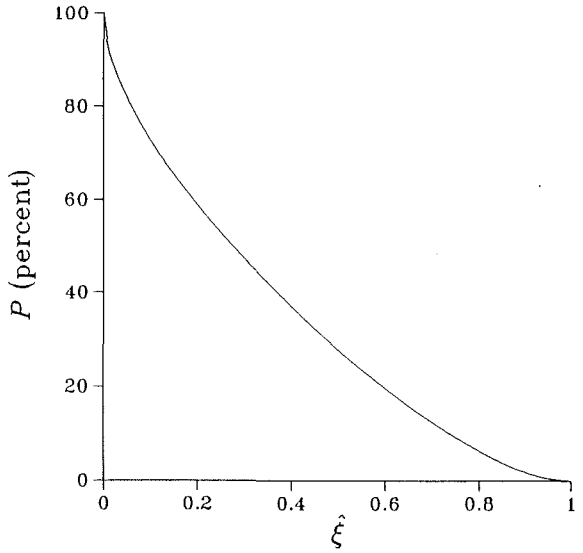

Fig. 8 Percentage P of all filaments in the contact region, located within the subregion $\hat{\xi} \leq \bar{\xi} \leq 1$, for $N = 500$ filaments, $t/r_h = 1.0$, and $\Delta = 0.508$ cm (0.2 in.)

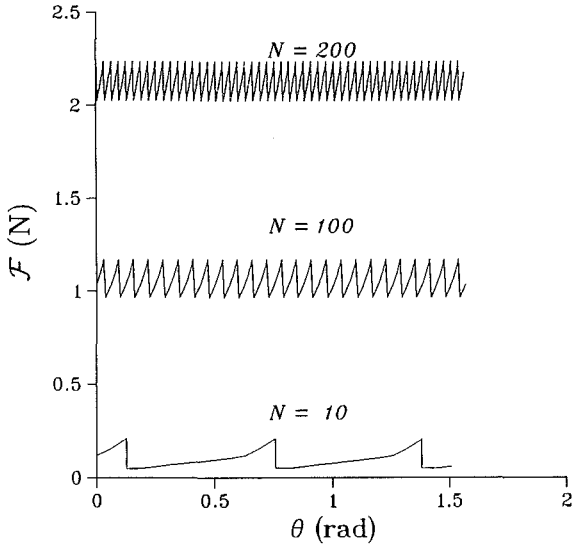

Fig. 10 Resultant force $\mathcal{F}$ vs. hub position θ for various numbers of filaments N with $\Delta = 0.508$ cm (0.2 in.)

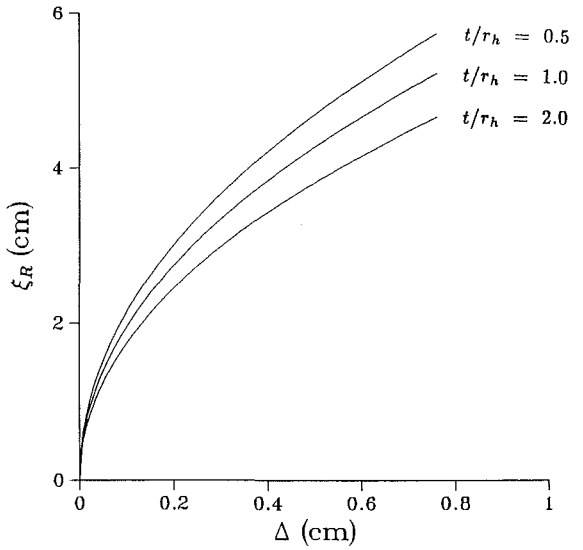

Fig. 9 Length of filament contact zone ξ_R vs. penetration depth Δ, for $t/r_h = 0.5$, 1.0, and 2.0 with $N = 500$ filaments

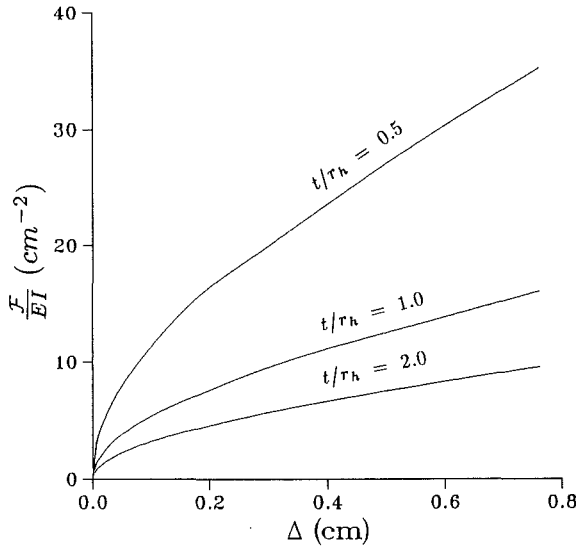

Fig. 11 Brush force $\mathcal{F}/EI$ vs. brush penetration depth Δ, for $t/r_h = 0.5$, 1.0, and 2.0 with $N = 500$ filaments

contact region is most rapid for small penetration depths. As the displacement is increased, however, an essentially linear relationship between the contact zone size and penetration depth is noted. In addition, for constant penetration depth, a reduction of the brush geometric parameter t/r_h, yields a corresponding increased contact zone.

Rotation of a brush having equispaced filaments yields a successive contact and release of the wires along ξ. The change of the resultant force $\mathcal{F}$, associated with the hub rotation θ, is examined in Fig. 10 for $\Delta = 0.508$ cm (0.2 in.), with $N = 10$ filaments, 100 filaments, and 200 filaments. The numerical solutions show that brushes having a greater number of equispaced filaments yield a corresponding increase in the resultant force. However, the magnitude of the force oscillation is associated with the periodic filament release from the workpart surface S, and therefore remains unchanged. In the case of a brush system having nonuniform filament distribution along the circumferential direction, it is anticipated that a more complex resultant force variation would be obtained. The magnitude of the filament release force would, nevertheless, remain unchanged.

In Fig. 11, the relationship between resultant force $\mathcal{F}/EI$ and brush penetration depth Δ is examined for $t/r_h = 0.5$, 1.0, and 2.0, with $N = 500$ filaments. A significant initial gradient is obtained for each response curve; however, as the displacement of the brush is increased, an essentially linear relationship between the resultant force and penetration depth is observed. A departure from this linear relationship would be anticipated if the filament material follows a nonlinear stress-strain law, or under a condition of severe deformation, whereby lateral contact is established between the filament and the workpart.

Brush stiffness is illustrated in Fig. 12 for penetration depth $0 \leq \Delta \leq 0.762$ cm (0.3 in.). Evaluation of brush stiffness K/EI is based upon equation (16) in conjunction with the data given in Fig. 11. A rapid decline of the initial stiffness is noted for each of the response curves. At larger penetration depths, however, an approximately constant brush stiffness is obtained.

5 Summary and Conclusions

A mechanics-based procedure has been developed for

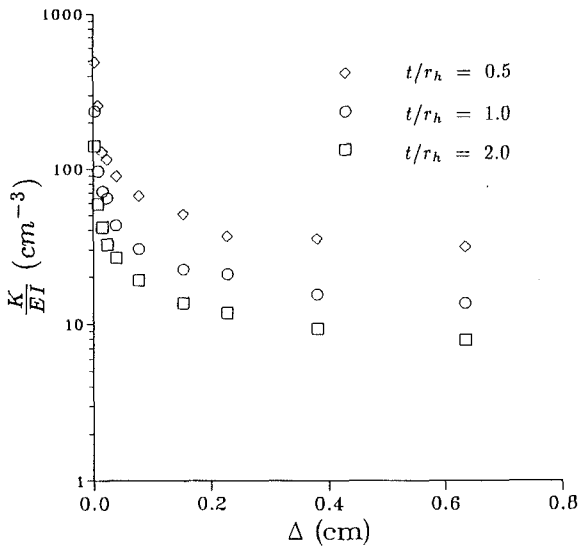

Fig. 12 Brush stiffness K/*EI* vs. brush penetration depth Δ, for t/r_h = 0.5, 1.0, and 2.0 with *N* = 500 filaments

evaluating constrained filament deformation and stiffness properties of filamentary brushes. Workpart forces developed within the contact zone are evaluated on the basis of an incremental numerical solution for filament contact with a flat, smooth surface. A numerical solution obtained on the basis of the present research is in excellent agreement with the corresponding result computed by post-buckling analysis. In addition, the size of the contact zone is independently computed by employing large deformation column analysis, and excellent agreement is obtained with the results predicted by the incremental solution procedure. The deformed configuration of the filament is reported to be independent of the flexural rigidity *EI*; filament tip force, however, is noted to vary in direct proportion with the flexural rigidity. Stiffness properties for wire brush systems are evaluated for several different geometries by superposing the individual filament-workpart contact forces.

An extension of the analytical work is presently being conducted for the purpose of examining the influence of friction and workpart curvature on filament deformation and brush stiffness properties. In addition it is recommended that an experimental research plan be developed which can provide basic information concerning the range of applicability of the analytical results presented in this study.

6 Acknowledgments

The authors gratefully acknowledge contributions made by Dr. Nicholas Nigro, Professor of Mechanical Engineering at Marquette University. This research was sponsored in part by the Milwaukee Brush Manufacturing Company under M. U. Grant 5966. Valuable discussion with Mr. James Henderson, Director of Engineering at the Milwaukee Brush Mfg. Co., is gratefully acknowledged.

7 References

1 Bisshopp, K. E., and Drucker, D. C., 1945, "Large Deflections of Cantilever Beam," *Quarterly of Applied Mathematics*, Vol. 3, pp. 272–275.

2 Chajes, A., 1974, *Principles of Structural Stability Theory*, Prentice-Hall, Inc., Englewood Cliffs, New Jersey, pp. 22–28.

3 Chapra, S. C., and Canale, R. P., 1985, *Numerical Methods for Engineers with Personal Computer Applications*, McGraw-Hill, Inc., London, pp. 496–497.

4 FitzPatrick, P. R., and Paul, F. W., 1987, "Robotic Finishing Using Brushes – Material Removal Mechanics," *SME Proceedings, Deburring and Surface Conditioning '87*, Phoenix, Arizona, MR87-156.

5 Gere, J. M., and Timoshenko, S. P., 1984, *Mechanics of Materials*, Second Edition, Wadsworth, Inc., Belmont, California, pp. 351–355, pp. 414–415.

6 Hamming, R. W., 1959, "Stable Predictor-Corrector Methods for Ordinary Differential Equations," *Journal of the Association of Computing Machinery*, Vol. 6, pp. 37–47.

7 Mitchell, T. P., 1959, "The Nonlinear Bending of Thin Rods," *Journal of Applied Mechanics*, Vol. 26, *Transactions of the ASME*, Series E, Vol. 81, pp. 40–43.

8 Paul, F. W., and FitzPatrick, P. R., 1986, "Robotic Controlled Brush Finishing," *ASME Symposium Volume*, pp. 101–107.

9 Seide, P., 1984, "Large Deflections of a Simply Supported Beam Subjected to Moment at One End," ASME *Journal of Applied Mechanics*, Vol. 51, pp. 519–525.

10 Timoshenko, S. P., and Gere, J. M., 1961, *Theory of Elastic Stability*, Second Edition, McGraw-Hill, Inc., London, pp. 76–81.